

# Reference frame access under the effects of great earthquakes: a least squares collocation approach for non-secular post-seismic evolution

D. D. Gómez<sup>1,2</sup> · D. A. Piñón<sup>2,3</sup> · R. Smalley Jr.<sup>1</sup> · M. Bevis<sup>4</sup> · S. R. Cimbaro<sup>2</sup> · L. E. Lenzano<sup>5,6</sup> · J. Barón<sup>5</sup>

Received: 20 April 2015 / Accepted: 11 November 2015  
© Springer-Verlag Berlin Heidelberg 2015

**Abstract** The 2010, (Mw 8.8) Maule, Chile, earthquake produced large co-seismic displacements and non-secular, post-seismic deformation, within latitudes 28°S–40°S extending from the Pacific to the Atlantic oceans. Although these effects are easily resolvable by fitting geodetic extended trajectory models (ETM) to continuous GPS (CGPS) time series, the co- and post-seismic deformation cannot be determined at locations without CGPS (e.g., on passive geodetic benchmarks). To estimate the trajectories of passive geodetic benchmarks, we used CGPS time series to fit an ETM that includes the secular South American plate motion and plate boundary deformation, the co-seismic discontinuity, and the non-secular, logarithmic post-seismic transient produced by

the earthquake in the *Posiciones Geodésicas Argentinas* 2007 (POSGAR07) reference frame (RF). We then used least squares collocation (LSC) to model both the background secular inter-seismic and the non-secular post-seismic components of the ETM at the locations without CGPS. We tested the LSC modeled trajectories using campaign and CGPS data that was not used to generate the model and found standard deviations (95 % confidence level) for position estimates for the north and east components of 3.8 and 5.5 mm, respectively, indicating that the model predicts the post-seismic deformation field very well. Finally, we added the co-seismic displacement field, estimated using an elastic finite element model. The final, trajectory model allows accessing the POSGAR07 RF using post-Maule earthquake coordinates within 5 cm for ~91 % of the passive test benchmarks.

**Electronic supplementary material** The online version of this article (doi:10.1007/s00190-015-0871-8) contains supplementary material, which is available to authorized users.

✉ D. D. Gómez  
ddgomez@memphis.edu

- <sup>1</sup> Center for Earthquake Research and Information, The University of Memphis, 3890 Central Ave, Memphis, TN 38152, USA
- <sup>2</sup> Dirección de Geodesia, Instituto Geográfico Nacional, Avda. Cabildo, 381 C1426, AAD, Ciudad Autónoma de Buenos Aires, Republic of Argentina
- <sup>3</sup> RMIT University, 402 Swanston St, Melbourne, VIC 3000, Australia
- <sup>4</sup> School of Earth Sciences, Ohio State University, 281 W. Lane Ave., Columbus, OH 43210, USA
- <sup>5</sup> International Center for Earth Sciences (ICES), Centro Universitario, Universidad Nacional de Cuyo, Mendoza, Mendoza Province, Republic of Argentina
- <sup>6</sup> Instituto Argentino de Nivología, Glaciología y Ciencias Ambientales (IANIGLA) CONICET, Universidad Nacional de Cuyo, Mendoza, Mendoza Province, Republic of Argentina

**Keywords** Least squares collocation · Earthquake deformation field interpolation · GPS · Reference frames · Time-dependent positioning

## 1 Introduction

In traditional geodesy and surveying, reference frames (RF) were realized using a combination of astronomical, trilateration and triangulation observations that resulted in apparent fixed benchmark coordinates due to the low precision of such observations. With the advent of high precision GPS surveying, we can no longer assume benchmark coordinates are fixed, since GPS can easily observe secular plate motions. The precision available from GPS/GNSS surveying therefore requires taking the observed motions into account by additionally stating both the epoch of the RF definition and the secular velocity of each benchmark. With the continuing improvements of GNSS technology, additional secular

and non-secular crustal deformation signals such as plate boundary deformation, co-seismic static offsets, years long post-seismic deformations, and glacial isostatic adjustment have also become observable and must be taken into account to produce very stable RFs (Bevis and Brown 2014). Co-seismic offsets, estimated using GPS measurements, range from  $\sim 10$  m in the rupture zone to several millimeters at distances  $>1000$  km for subduction megathrust (Mw9+) earthquakes (Pollitz et al. 2011). Such earthquakes also produce post-seismic deformations that can occur for decades before returning to the secular inter-seismic deformation component of the earthquake cycle (Khazaradze et al. 2002; Zweck et al. 2002; Hu et al. 2004; Wang et al. 2007). The description of the time evolution of a CGPS station's position, therefore, must take all these effects into account and can be described using an extended trajectory model (ETM) (Bevis and Brown 2014).

Estimation of a passive benchmark's position at a given epoch, which allows accessing the RF, can be made through interpolation, such as least squares collocation (LSC), if the number and density of observations suffice and the velocity or deformation field is sufficiently smooth (Gómez et al. 2015), or using geodynamics-based results such as finite element (FEM) or analytic models (Tong et al. 2010; Lorito et al. 2011; Pollitz et al. 2011; Moreno et al. 2012; Snay et al. 2013; Lin et al. 2013). To estimate passive benchmark positions at a given epoch in South America in the Geocentric Reference System for the Americas (*Sistema de Referencia Geocéntrico para las Américas*, SIRGAS) RF (Seemüller et al. 2009) one can use the existing Velocity Model for SIRGAS (VEMOS2009) (Drewes and Heidbach 2012) that only considers plate motion and boundary deformation, both of which are secular.

The 2010 (Mw 8.8) Maule, Chile, earthquake, in the region spanning  $28^{\circ}\text{S}$  to  $40^{\circ}\text{S}$  and extending from the Pacific to the Atlantic oceans, produced large, static, co-seismic displacements and an ongoing deformation associated with non-secular after-slip and visco-elastic relaxation that will last for decades. The coordinates of the stations in the RF, therefore, suffered both a large jump on the day of the earthquake, and a large, non-secular change in their trajectories. Due to these effects, the secular VEMOS2009 model no longer provides useful estimates of passive benchmark trajectories, in the affected area, since it does not provide estimates of the co- and post-seismic deformation components.

Many geodetic and land surveying applications require passive benchmarks and CGPS station coordinates to be given in a specific RF and at a specific epoch, which in general is the epoch of the RF definition. In Argentina, the official RF is called *Posiciones Geodésicas Argentinas 2007* (POSGAR07), which is a densification of the International Terrestrial Reference Frame 2005 (ITRF05) (Altamimi et al. 2007). Its materialization was performed using measure-

ments between 2006 and 2007 and defined at the average measurement epoch 2006.632. When a new CGPS station or geodetic benchmark is installed at a location without pre-Maule earthquake measurements, determining the POSGAR07 coordinate (i.e., accessing the RF) is difficult, as there is no practical procedure to “remove” the co-seismic discontinuity and post-seismic deformation to obtain its epoch 2006.632 coordinate. Furthermore, before the Maule earthquake, positions in POSGAR07 of passive benchmarks were known with an accuracy of  $\sim 1\text{--}10$  cm. After the earthquake, the co-seismic displacements changed the accuracy of passive benchmark coordinates within the region affected by the earthquake. When using the POSGAR07 coordinates (those defined at epoch 2006.632), the accuracy of the passive network is now estimated to be  $\sim 10\text{--}70$  cm, depending on the size of the co-seismic displacement at the position of the benchmark. This level of accuracy is not sufficient for many applications such as civil engineering and land surveying. Moreover, the coordinates continue to change with undetermined trajectories, preventing access to the RF using observations obtained after the earthquake. This is especially problematic during regional geodetic network adjustments in the region with large horizontal displacements and strong post-seismic motions.

To obtain POSGAR07 coordinates starting from post-earthquake coordinates, or vice versa, it is therefore necessary to establish a model to access the RF. This model has to take into account all the effects produced by the Maule earthquake and provide continuous temporal and spatial estimates of benchmark trajectories. We will refer to this as a trajectory prediction model (TPM). The creation of a TPM to access the RF has broader implications than just the practical use of a terrestrial RF such as POSGAR07. During the past 20 years, the Central Andes GPS Project (CAP) has been collecting campaign GPS data throughout the central and southern Andes. For “historic” stations, i.e., GPS sites with at least two measurements before and one after the Maule earthquake, a model of the post-seismic deformation TPM provides additional information regarding the co-seismic displacements. We will show that the post-seismic deformation TPM models the positions/coordinates of campaign GPS data very well. The application of this model provides additional control on estimates of co-seismic displacement that can be used to constrain models of the earthquake and the tectonic evolution of the Andes.

Snay et al. (2013) also developed models to predict station coordinates under the effects of great earthquakes. Although our approach is similar, there are several significant differences in our proposed methodology. First, they used a dynamic model for the secular inter-seismic velocities, while we used the LSC approach of Drewes and Heidbach (2012). Another difference is the type of dynamic model used to estimate the co-seismic displacements. We

used a spherical FEM for the Maule earthquake, while [Snay et al. \(2013\)](#) used analytic dislocation theory in a half-space ([Okada 1985](#)). Finally, for post-seismic deformation, we propose a kinematic approach similar to that of [Snay et al. \(2013\)](#), but using a spatial taper function and LSC to model the first-order behavior of the observed post-seismic transients.

To obtain the TPM, we used CGPS data from the Argentine Continuous Satellite Monitoring Network (*Red Argentina de Monitoreo Satelital Continuo*, RAMSAC), CAP, the International GNSS Service (IGS), and several other scientific CGPS networks (see Supplementary Material). We used CGPS time series from the Argentine Scientific Processing Center (*Centro de Procesamiento Científico Argentino*, CPC-Ar) at the Argentine National Geographic Institute (*Instituto Geográfico Nacional*, IGN) for stations they process (all stations in Argentina, plus a handful of nearby IGS stations) and the Nevada Geodetic Laboratory daily solutions, published on-line, for other stations, mostly in Chile. We applied the ETM method of [Bevis and Brown \(2014\)](#) to the time series to obtain estimates of both the non-secular, post-seismic transients generated by the earthquake and the secular plate motion and inter-seismic velocities. Using CGPS stations installed after the earthquake and post-earthquake CAP campaign data, we will show that the standard deviations (95 % confidence level) for the north and east components of our post-seismic TPM are 3.8 and 5.5 mm, respectively. Finally, we use POSGAR's pre- and post-seismic measurements with a FEM of the co-seismic displacements to show that the TPM allows accessing POSGAR07, using post-seismic coordinates, within the original accuracies at ~91 % of the test benchmarks. Although this work presents a model that has been applied to CGPS and campaign data within Argentina, it can be used in any region with post-seismic deformation and a limited number of observations.

## 2 Underlying secular inter-seismic velocities of the CAP, RAMSAC and IGS GPS networks

[Bevis and Brown \(2014\)](#) present an ETM and demonstrate that its application to RF materialization can considerably reduce systematic errors in RF realization. In addition to the secular velocities used in constant velocity models (CVM), their ETM contains static offsets to model equipment changes and co-seismic jumps, sinusoidal components to model observed periodic displacements, and logarithmic transients to model non-secular after slip and visco-elastic relaxation. The linear mathematical expression for the ETM is:

$$\mathbf{x}(t) = \sum_{i=1}^{n_p+1} \mathbf{p}_i (t - t_R)^{i-1} + \sum_{j=1}^{n_j} \mathbf{b}_j H(t - t_j)$$

$$+ \sum_{k=1}^{n_F} [\mathbf{s}_k \sin(\omega_k t) + \mathbf{c}_k \cos(\omega_k t)] + \sum_{i=1}^{n_T} \mathbf{a}_i \log[1 + \Delta t_i / T_i] \quad (1)$$

where  $t$  is time,  $n_p$  is the number of polynomial terms,  $\mathbf{p}_i$  is the amplitude of the  $i$ th polynomial term and  $t_R$  is the reference epoch (adopted by convention). Using one polynomial term,  $n_p = 1$  provides a secular, or constant, velocity that describes plate motion and effects such as inter-seismic deformation. "Jumps", used to model equipment changes, earthquake co-seismic jumps, etc., are modeled using the Heaviside function,  $H$ , where  $n_j$  is the total number of jumps, with amplitude  $\mathbf{b}_j$  at time  $t_j$  for the  $j$ th jump. For the periodic component,  $n_F$  is the number of frequencies used, with the  $k$ th frequency being  $\omega_k$ . Phase is determined using both sine and cosine terms, with amplitudes  $\mathbf{s}_k$ ,  $\mathbf{c}_k$ . The final component models logarithmic transients. As with the jumps, a number of transients can be included,  $n_T$ . Each transient has its own amplitude,  $\mathbf{a}_i$  and a relaxation time  $T_i$ . For each  $i$  seismic event,  $\Delta t_i = 0$  for  $t < t_{EQ}$ , where  $t_{EQ}$  is the reference epoch of the earthquake, and  $\Delta t_i = t - t_{EQ}$  for  $t \geq t_{EQ}$  since the post-seismic transient exists only after  $t_{EQ}$ . [Bevis and Brown \(2014\)](#) provide an exhaustive description of the evolution of the trajectory models and how to select and apply the various components of the model.

To describe the CGPS trajectories, we used  $n_p = 1$ , since none of the time series display observable pre-seismic non-linearity, i.e., they are typical secular CGPS time series associated with plate motions and the regional plate boundary tectonics. Two frequencies, annual and semi-annual, are typically sufficient to model the observed periodic behavior and we used  $n_F = 2$  for these components. As would be expected from a least squares adjustment, the inclusion of additional parameters in the ETM (i.e., the periodic terms) reduces the misfit. This variance reduction in misfit, however, should be statistically significant to justify the inclusion of additional model parameters. To determine if the misfit reduction was significant, we applied an  $F$ -test to a set of ETMs from 37 CGPS stations with data from before and after the Maule earthquake, and found that only seven stations (BCAR, CHLT, JUNT, LHCL, LPGS, RWSN and SRLP) did not show a statistically significant improvement of the residuals' variance on any of their three components (although the misfits were always reduced). Analyzing the north, east and up components independently, we found statistically significant improvements in 24 stations for the north, 15 stations for the east and 18 stations for the up components.

The inclusion of periodic terms in most cases also helps to better constrain the adjustment of the ETM parameters. We compared the least squares estimated uncertainty of the velocity, co-seismic jump and logarithmic transient for the

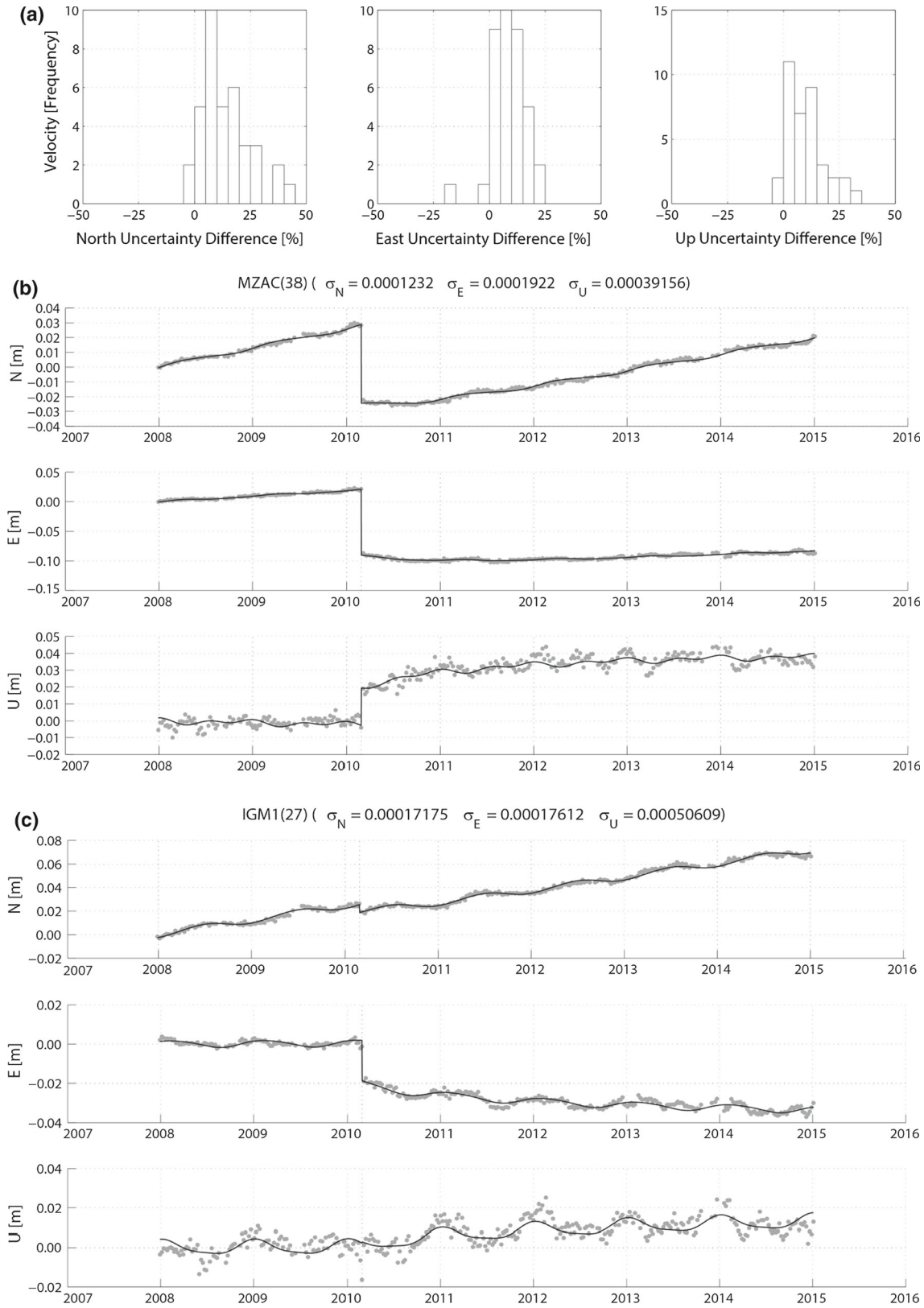


**Fig. 1** a North, east and up histograms of the least squares estimated uncertainty change (in percentage) for the velocity component of the ETMs with and without periodic terms. A positive value represents a decrease in uncertainty (precision increase). b ETM of RAMSAC sta-

tion MZAC. Co-, post- and inter-seismic components can be observed. c ETM of RAMSAC station IGM1. Periodic terms are more visible (compared to MZAC) since the scales of the co-seismic jumps are smaller than those from MZAC

ETM both with and without periodic terms. From the estimated uncertainties, Fig. 1a shows the north, east and up histograms of the percentage change in the uncertainty of the velocity estimate. In these plots, a positive percentage change represents a precision increase (uncertainty reduction) with respect to the precision of the ETM without the periodic terms. For three stations examined, we observe an increase in precision of up to 40–45 %, although most of the increases are less than 25 %. There are only two cases where we observe a precision decrease in the north velocity estimate (stations RWSN and SJAV), two stations in the east velocity estimate (COYQ and SJAV) and two stations in the up velocity estimates (SJAV and VAL3), although we only note one considerable reduction in the east component for station SJAV of  $\sim 16$  %. We also note that the mean uncertainty (95 % confidence level) for the three velocity components varies between 0.4 and 1.4 mm/year, which make these changes (positive or negative) very small. Histograms for the other two parameters (co-seismic jump and logarithmic transient) show very similar distributions and are therefore not shown.

To model the logarithmic post-seismic transients from the Maule earthquake, we applied a value of  $T_i = 0.5$  years for the relaxation time of all the CGPS time series. This is different from the value  $T_i = 1$  year proposed by Bevis and Brown (2014). In general, the logarithmic transient adjustment is relatively insensitive to the exact value of  $T$ , and we found that using  $T_i = 0.5$  allowed use of a single relaxation time for the whole network while providing a good fit for both the near and far field post-seismic time series.

One of the features of the ETM is that the least squares adjustment is done in a single step, without breaking the model into pre- and post-seismic adjustments. If a sufficient number of pre-seismic observations exist, estimation of the secular component is dominated by the pre-seismic part of the time series. To obtain a stable secular velocity, we only used time series with more than  $\sim 2$  years of pre-earthquake data. This provides a robust estimate of the CGPS stations' underlying inter-seismic velocities, which are assumed to remain constant throughout the earthquake cycle. Figure 1b and c shows two examples of the ETM adjustment for RAMSAC stations MZAC, located in the near field of the Maule earthquake (Mendoza, Argentina), and IGM1, located in the far field (Buenos Aires, Argentina), both of which have  $\sim 2$  years of pre-earthquake data. These plots show the three components (north, east and up) although the TPM developed does not include the vertical component.

Drewes and Heidbach (2012) noted that vertical signals are much more complex and are very difficult to model using either interpolative (e.g., LSC) or numerical models, and therefore, we also only model the horizontal components, although Snay et al. (2013) estimated both horizontal and vertical components using numerical modeling and obtained very good results. The selection of LSC to produce our TPM

was made based on the fact that the LSC approach is much simpler to implement than numerical models, and provides equally good results (Drewes and Heidbach 2012), nevertheless, this selection comes at the expense of not modeling the vertical component.

To estimate the inter-seismic velocities, we developed an LSC interpolation to estimate the velocity field on a  $1^\circ$  grid. To apply LSC, we first remove plate motions using the ITRF compatible, no-net-rotation (NNR), Actual Plate Kinematic Model (Drewes 2009). The problem of estimating an empirical covariance function for inter-seismic velocities has been described by Drewes and Heidbach (2012). They show that correlation lengths for the north and east velocity components are quite different in regions suffering crustal deformation (e.g., the Andes cordillera) than in stable South America (e.g., the east coast). The empirical covariance functions are therefore estimated using a point by point calculation, as in Drewes and Heidbach (2012). We proceeded as follows. For each point for which velocity is to be estimated (1) we perform a Delaunay triangulation over the set of vertices consisting of the CGPS stations plus the point of interest, (2) we then select only those triangles that include the point of interest, (3) using only the CGPS stations from step 2 with pre-earthquake data, we estimate the empirical covariance function, (4) we apply LSC at the point of interest using this empirical covariance function and the detrended CGPS inter-seismic velocities.

Figure 2a shows the velocity model, known as the “linear Argentine Velocity” model (*Velocidades Argentinas Lineales*, Vel-Ar-Lin), obtained using this procedure. We also compare Vel-Ar-Lin against VEMOS2009 (Fig. 2b), which shows that their difference never exceeded 8 mm. The largest differences are in Patagonia (Río Negro, Chubut and Santa Cruz Provinces), where we used additional CPGS stations that were not available in the preparation of VEMOS2009. A few large differences can be observed near the edges of Vel-Ar-Lin (in Bolivia and west from Tierra del Fuego) but these areas are outside the intended limits of the model. Note that in this version of Vel-Ar-Lin, we are not considering the deformation associated with the South America—Scotia plate boundary across the Magallanes–Fagniano transform fault in Tierra del Fuego. This improvement will be taken into account in future versions of Vel-Ar-Lin.

### 3 Least squares collocation of post-seismic deformation

To obtain an estimate of the amplitude of the post-seismic signal, we need to add the logarithmic transients to the secular, inter-seismic velocity field. The ETM of the CGPS time series provide point measurements of the transient amplitude components at the location of the CGPS stations. These point

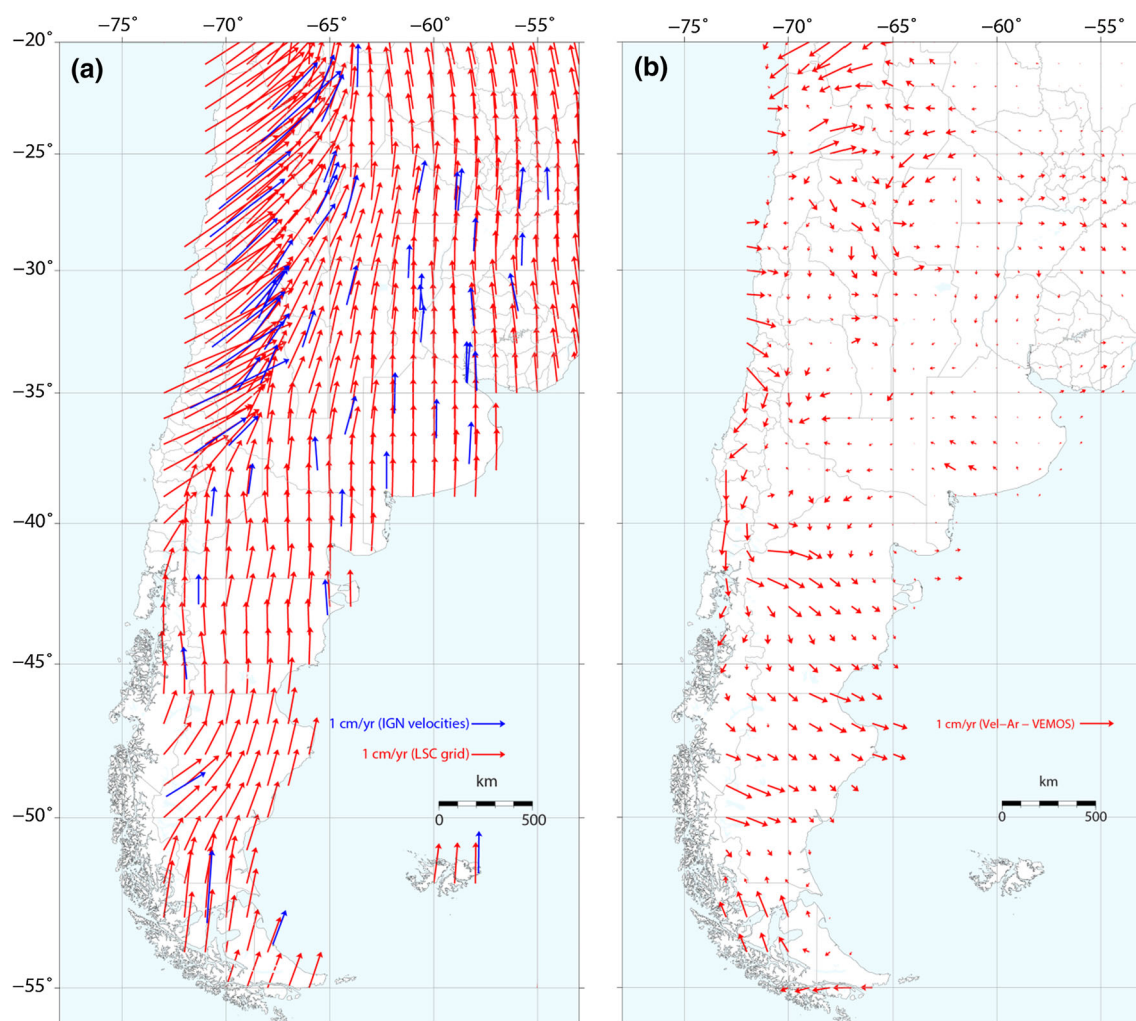


**Fig. 2** **a** Least squares collocation of the secular inter-seismic velocities of the RAMSAC, CAP and IGS networks in POSGAR07. *Blue arrows* show the CGPS stations used for the interpolation. *Red arrows* show the  $1^\circ$  grid in latitude and longitude of interpolated velocities. **b**

Residual of the difference between Vel-Ar-Lin and VEMOS2009 velocity model. Due to the addition of new CGPS sites, the largest differences are located in Patagonia

measurements will be interpolated using an LSC to obtain a spatially continuous logarithmic transient field.

Within a few weeks of the Maule earthquake, the CAP group installed several dozen CGPS stations in and around the epicentral area in Chile and Argentina, while also reoccupying existing campaign sites and installing new ones (in Argentina only) to densify sampling of the post-seismic deformation field. As previously discussed, the ETM assumes that the secular velocity associated with plate motion and plate boundary interaction deformation is constant throughout the earthquake cycle, even after the post-seismic deformation starts. Unfortunately, as the basis functions of the secular and logarithmic transient components of the ETM are not orthogonal, we cannot constrain the secular and logarithmic components of the ETM simultaneously. Therefore, we need a sufficiently long pre-earthquake

time series to independently constrain the secular component.

To include the new, post-earthquake only, CGPS stations in the post-seismic deformation model, we removed their motion under the Vel-Ar-Lin model before adjusting for the post-seismic component of the ETM (see Supplementary Material). The transients estimated using this procedure are compatible with those estimated for CGPS stations with pre-earthquake data and can, therefore, be included into a single LSC interpolation for the logarithmic transient amplitudes. Adding this transient interpolation to Vel-Ar-Lin, we obtain one of the TPM components necessary to access POSGAR07 coordinates based on the measured post-seismic coordinates (less the component due to the co-seismic displacement that will be discussed later).

To apply LSC to a data set, it must meet the intrinsic hypothesis (Ligas and Kulczycki 2010; Vieira et al. 2010), which in its simplest and most often used form requires that the data do not exhibit a trend. There are few restrictions on the function used to remove the trend, although in practice, low-order polynomials are oftentimes used. The quality of the trend removal can be tested with a semi-variogram, which displays a sill near the expectation value of the detrended data (Vieira et al. 2010). Following Vieira et al. (2010), we detrended the data using polynomials of increasing degree, until the semi-variogram displayed a stable sill. We found that a degree four polynomial adequately removed the post-seismic transient trend, but produced undesired edge effects near the model limits. Further examination of the post-seismic deformation field, however, showed that as we move away from the rupture zone, amplitudes of the transient fall to near zero with a decaying exponential shape. We therefore used spatial exponential tapers, one for the E–W and one for the N–S trends, respectively, that provide a first-order approximation to the trend of the data, while also decaying to zero as we move away from the rupture zone. The detrending function is:

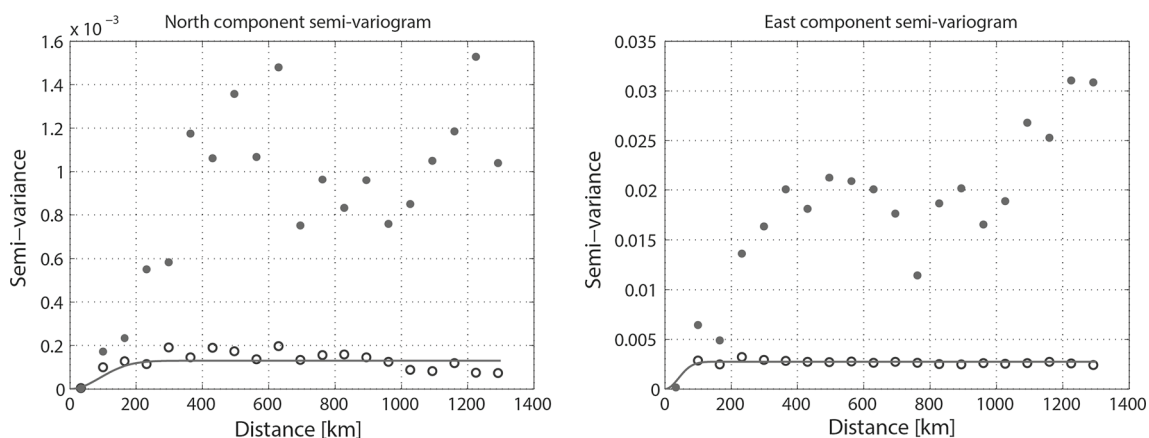
$$A = a \exp\left(-\frac{(x - x_0)^2 + (y - y_0)^2}{2\sigma}\right) \quad (2)$$

where  $x_0$ ,  $y_0$  is the origin of the taper,  $a$  is the maximum amplitude and  $\sigma$  is the decay distance. We found the best fitting parameters  $x_0$ ,  $y_0$ ,  $a$  and  $\sigma$  for the north and east components of the transients by performing a grid search over the space of residuals produced by (2).

From Fig. 3, we note that it is possible to apply LSC to the detrended data, since the semi-variograms show a stable sill after removing the trend. The stability of the sill also shows that the data can be modeled as a stationary process, which means that we can use a single covariance function for the

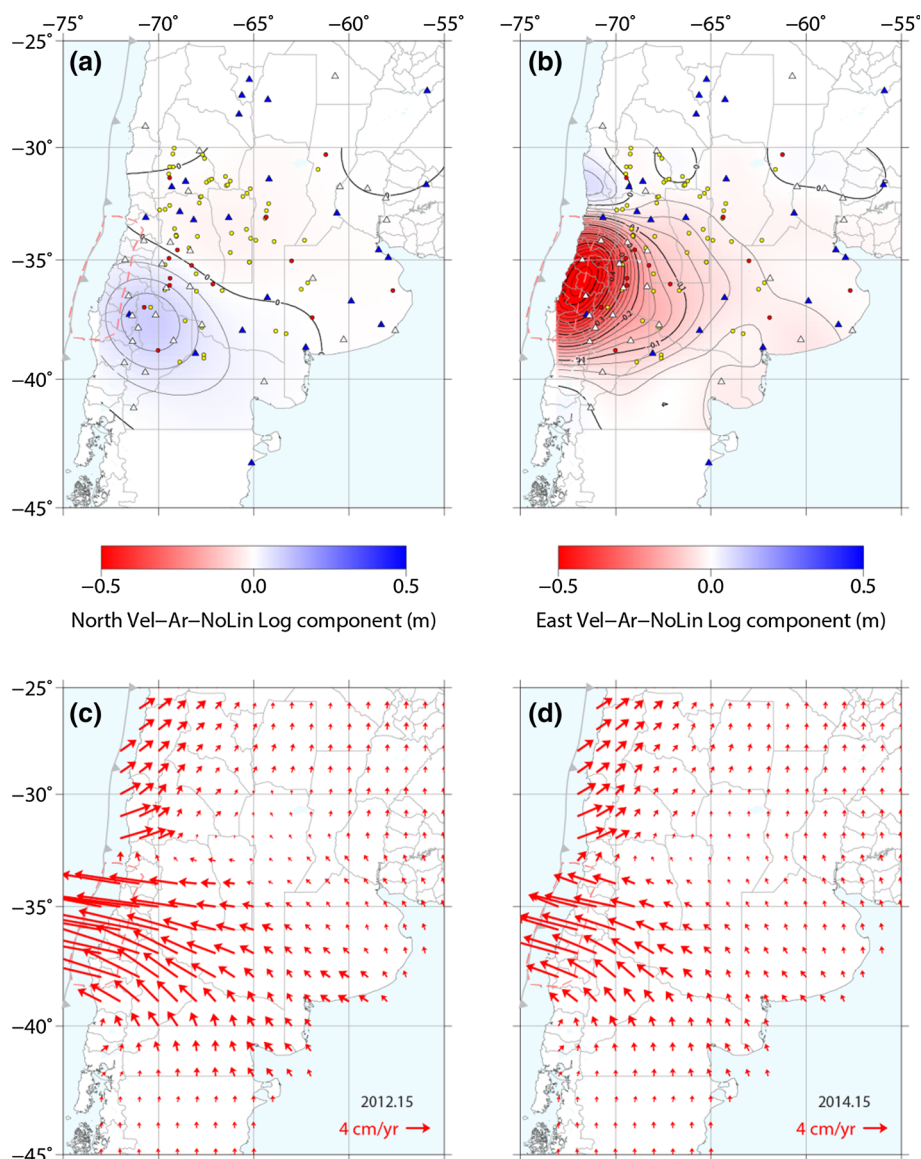
entire domain. Therefore, we applied the LSC method to the logarithmic transients to produce a  $0.25^\circ$  grid. This spacing was selected so the transient data between grid nodes can be linearly interpolated, which simplifies using the model. The spacing was verified by comparing the transients obtained from the ETMs against the transients obtained by linearly interpolating the post-seismic deformation LSC model. A larger grid spacing (say,  $1^\circ$ ) would produce interpolated transients that are not in agreement with the observed data, due to the non-linearity of the spatial change of the logarithmic transients.

Figure 4a and b shows the LSC interpolated logarithmic amplitudes (in meters), which we have called “Argentine Non-Linear Velocities” (*Velocidades Argentinas No Lineales*, Vel-Ar-NoLin), while Fig. 4c and d shows two snapshots of the instantaneous velocity field (in cm/year) 2 and 4 years after the earthquake (epochs 2012.15 and 2014.15). To test Vel-Ar-Lin and Vel-Ar-NoLin, we examined the residuals calculated by subtracting the LSC estimated positions from observed time series for a set CAP campaign and CGPS sites that were not included in the development of the LSC models (sites indicated by red circles in Fig. 4a and b). We fit normal distributions to the residual histograms (Fig. 5a and b) where we found standard deviations (95 % confidence level) of 3.8 and 5.5 mm in the north and east components, respectively. A slight tendency towards negative values can also be observed, which reveals the presence of a small systematic bias that is probably due to the misfit of the logarithmic transient to the data, observed during the first month after the earthquake. Bevis and Brown (2014) showed this misfit can be reduced by adjusting the value of the relaxation time for each time series. As discussed earlier, we did not apply this procedure since we used a common relaxation time for the entire network. For the precision and purposes of the model developed here, however, these misfits can be ignored.



**Fig. 3** Semi-variogram plots of the north and east components of the post-seismic transient after applying an exponential taper detrending function. Empty circles show the detrended data, filled circles show the original data, and the solid line is the Gaussian semi-variance model

**Fig. 4** Least squares collocation model of the logarithmic transients for **a** north and **b** east components. *Blue triangles* show the CGPS stations that have  $\sim 2$  or more years of pre-earthquake data. *White triangles* show CGPS that do not meet the condition to be included in the Vel-Ar-Lin estimation. *Red circles* show the test stations, which have multiple measurements, used to verify the quality of the Vel-Ar-Lin and Vel-Ar-NoLin models. *Yellow circles* are POSGAR benchmarks with only one measurement before and one after the earthquake. Contours of logarithmic transients every 0.025 m. *Red dashed line* shows the 2010 Maule earthquake rupture zone as defined by aftershocks. **c** Snapshot of the instantaneous velocity field at epoch  $\sim 2012.15$ . **d** Same as **c** at epoch  $\sim 2014.15$



#### 4 Accessing POSGAR07 using post-seismic coordinates: co-seismic displacements

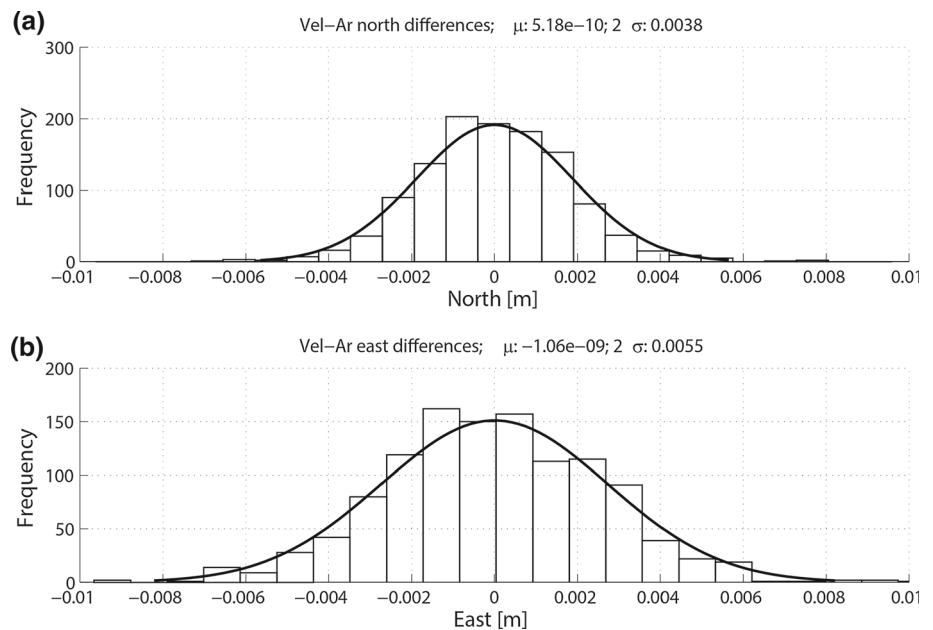
To successfully access POSGAR07 using post-seismic coordinates, a co-seismic displacement model must also be included. This model, combined with the secular and non-secular LSC models (Vel-Ar-Lin and Vel-Ar-NoLin) results in the final, complete TPM “Argentine Velocities” (*Velocidades Argentinas*, Vel-Ar) connecting the post-seismic coordinates to the pre-seismic coordinates.

Immediately after the Maule earthquake (between epochs 2010.2 and 2010.9), teams from CAP and IGN performed measurements on  $\sim 60$  existing CAP and POSGAR benchmarks (see Supplementary Material) to quantify the co-seismic displacement and begin measurements of the post-seismic deformation. Based on results of the immediate

post-earthquake campaign, IGN produced a set of recommendations for land surveyors operating in the region suffering deformation due to the Maule earthquake. Although most land surveyors do not use scientific GPS processing software to determine coordinates, the crustal deformation effects of the Maule earthquake are large enough, especially in the Provinces of Mendoza and Neuquén, that even with commercial GPS processing software application of Vel-Ar TPM is necessary to estimate coordinates that are within the working tolerances of the original network.

As with the plate velocity, inter-seismic and post-seismic signals, there are two general methods to estimate the co-seismic displacements at a non-CGPS benchmark: (1) kinematic model method: interpolate from nearby sites with CGPS measurements or (2) dynamic model method: use a physical/geodynamic model for the crustal deformation

**Fig. 5** Histogram of the difference between the modeled and observed trajectories and their fits to normal distributions for **a** north and **b** east components, for CAP and RAMSAC CGPS sites and CAP campaign sites with multiple measurements used in the Vel-Ar-Lin and Vel-Ar-NoLin test



effects generated by the earthquake. LSC, an example of interpolation in a kinematic model, has previously been applied, highly successfully, to model secular plate motions and inter-seismic deformations, and we have extended it here to also model post-seismic transients. Geodynamic models can be analytic solutions or numerical models such as FEM. In the case of using LSC to interpolate the co-seismic static offset for the Maule earthquake, Gómez et al. (2015) showed that due to the small number of CGPS stations and the rapid variation of the co-seismic displacement field, especially in the near field, an LSC of the co-seismic offset dataset does not produce an adequate interpolation. Although it has been suggested to use the LSC post-seismic and inter-seismic models to estimate the co-seismic displacements at sites with a few observations before and after the earthquake (Drewes and Sánchez 2013), this method only provides indirect, unverifiable estimates, with unknown precision, of the co-seismic displacement field. We have therefore estimated the co-seismic displacements with a FEM using Pylith (Aagaard et al. 2013). FEM is a numerical technique for finding approximate solutions to differential equations. Pylith, one of many programs available to compute finite element solutions, is a numerical approach to solve dynamic and quasistatic elasticity problems. We will later show that the FEM model satisfies our target precision.

FEM is one of the many classes of solutions to geodynamic models. For example, Snay et al. (2013) applied dislocation theory to a flat earth model to quantify the co-seismic displacements of 29 major earthquakes that produced co- and post-seismic deformation in and around the United States. As the region affected by the Maule earthquake, studied here, extends from Chile to eastern Argentina, a flat earth or half-

space model is inappropriate and we therefore used a layered spherical FEM with Preliminary Earth Model (Dziewonski and Anderson 1981) layer thicknesses and elastic properties. Although we used a FEM, a spherical analytical solution to the problem is also available from Pollitz (1996) that has been applied to the Maule earthquake (Pollitz et al. 2011).

The construction of a FEM starts by defining a mesh of nodes to which the finite element method will be applied. This mesh or grid of nodes is, in general, not a uniformly sampled domain, since the mesh is a discretization of the modeled geometry and, therefore, the spacing and shape of the figures formed by the FEM nodes changes to adapt to the model geometry. The FEM used for Vel-Ar is an ongoing project of the CAP group and only includes the first-order geometrical characteristics that have the greatest impact on estimating co-seismic deformation. It uses triangular elements and has an approximate spacing of 30 km between nodes, although in the near field (where the co-seismic displacements are less smooth) the spacing averages  $\sim 20$  km.

After the model geometry is defined, which includes both earth structure and properties and an a priori fault geometry, the GPS data are used to invert for a finite fault slip model. The input data for the finite fault slip model least squares inversion are the co-seismic jumps obtained from the ETMs. The design matrix used to solve the least squares problem is formed by the so-called Green's functions or impulse responses of the CGPS sites obtained from the FEM, and a discrete smoothing operator (Maerten 2005). The inversion yields the approximate slip distribution on the predefined fault surface that we defined by the USGS South American subduction zone slab model (Hayes et al. 2012). Once the finite fault slip model is obtained, we run a forward calcu-

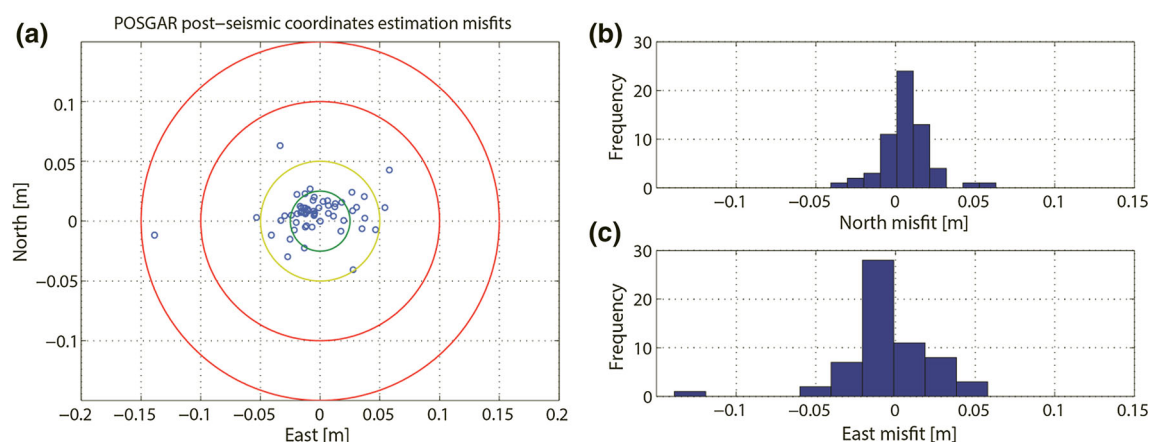


**Fig. 6** **a** Misfit between the post-seismic measurements of POSGAR benchmarks. *Green, yellow and red circles* represent a misfit distance of 2.5, 5, 10 and 15 cm. Test sites are shown in Fig. 4a and b by *yellow filled circles*. **b** Histogram of north component differences shown in **a**. **c** Histogram of east component differences shown in **a**

lation to estimate the co-seismic displacements at each node of our FEM. Finally, we extract the co-seismic displacement information from the nodes located on the surface of the FEM.

We tested the ability of the TPM to access POSGAR07 using the POSGAR sites that were not used in the calculation of Vel-Ar (Fig. 4a and b, yellow filled circles). Using the pre-seismic coordinates (obtained between epochs 2006 and 2007.5), we applied Vel-Ar-Lin and Vel-Ar-NoLin to estimate the inter-seismic and post-seismic displacements at the POSGAR benchmark sites and the jumps obtained from the FEM co-seismic model to estimate the total displacement and added this to the RF definition coordinate to obtain the estimate of the post-seismic coordinate. Finally, we compared the predicted post-seismic coordinate to the post-seismic measurement. The misfits in the north and east components are shown in Fig. 6a, where we note that 38 of 60 sites ( $\sim 63\%$ ) fall inside the 2.5 cm limit, 17 ( $\sim 28\%$ ) fall between 2.5 and 5 cm, and 5 ( $\sim 8\%$ ) fall outside the 5 cm limit. Only one measurement falls outside the 10 cm limit (with a misfit of 13.8 cm), although we do not discard the possibility of a blunder in the measurement or processing of that site. Figure 6b and c shows the histograms of the misfits shown in Fig. 6a, where we note a systematic bias in both the north and east components, respectively. These biases are a result of the misfit between the FEM and the observed co-seismic displacements.

## 5 Conclusion

We have shown how to use the post-seismic logarithmic transients, estimated using an ETM, to produce a LSC model of the post-seismic deformation field of the 2010, (Mw8.8), Maule earthquake. As our focus is the region affected by the Maule earthquake, we produced our own, updated, inter-

seismic velocity model (Vel-Ar-Lin), using more CGPS data within Argentina than was available during the creation of VEMOS2009. This methodology we developed can be used to update VEMOS2009 to include the effects of the Maule earthquake by incorporating a logarithmic transient LSC model and a co-seismic displacement model. Updating VEMOS2009 in this manner would allow it to predict the trajectories of the passive benchmarks in the SIRGAS RF using a non-linear-model (*modelos no lineales*, MoNoLin), without having to break the time series into multiple, sequential, linear segments, with periodic updates, as proposed by Drewes and Sánchez (2014).

Our results show that  $\sim 63\%$  of the test sites (i.e., those not used to produce Vel-Ar; Fig. 4a, b) have misfits less than 2.5 cm and  $\sim 28\%$  have misfits between 2.5 and 5 cm (Fig. 6a). The application of Vel-Ar TPM to provincial geodetic benchmark networks will provide access to POSGAR07 with an accuracy that is approximately the same as that of the POSGAR network before the earthquake occurred. Examining the estimated precision of the post-seismic deformation estimates (Fig. 5a and b), we conclude the majority of the misfit in the POSGAR benchmark test is due to the co-seismic model, not the post-seismic LSC model (Vel-Ar-NoLin). Nevertheless, the FEM developed by Gómez et al. (2015) produces a much better fit than an LSC of the co-seismic displacement field and we therefore selected the FEM to estimate the co-seismic displacement field. A finite element model is currently under development by the CAP geodynamics group for both the co-seismic and post-seismic components. IGN is currently developing a legal implementation of the Vel-Ar TPM that will be available from their website.

While the method presented here successfully provides trajectory estimates of passive and CGPS sites after the Maule earthquake, it requires at least 2 years of observations to correctly constrain the post-seismic deformation (Bevis and

Brown 2014). This kinematic approach is therefore reasonable to produce a TPM for an earthquake that occurred five years ago. In the case of future great earthquakes, dynamic models, as in Hu et al. (2004), could provide immediate estimation of the deformation field without waiting for months to years to measure and fit the post-seismic effects. Such dynamic models should be considered for immediate post-earthquake surveying activity and future TPM developments.

**Acknowledgments** We thank Hernán Guagni, Agustín Raffo and the Department of Geodesy of the IGN for providing the GPS processing and additional support. We thank Benjamin Brooks and James Foster for providing additional GPS data used in this work and Wolfgang Schwanghart for providing his semi-variogram code through the Matlab File Exchange. The authors would also like to thank three anonymous reviewers for their insightful comments and suggestions that have contributed to improve this paper. This work was supported by the NSF Collaborative Research: Great Earthquakes, Megathrust Phenomenology and Continental Dynamics in the Southern Andes, award number EAR-1118241, and the Center for Earthquake Research and Information, University of Memphis. *Data sources* Pylith web page: <http://geodynamics.org/cig/software/pylith/>. Maps were made using the Generic Mapping Tools version 5.1.1 (Wessel and Smith 1998). Additional publicly available time series of CGPS stations located in Chile (and that are not part of CPC-Ar) were obtained from the Nevada Geodetic Laboratory: <http://geodesy.unr.edu/>.

## References

- Aggaard BT, Knepley MG, Williams CA (2013) A domain decomposition approach to implementing fault slip in finite-element models of quasi-static and dynamic crustal deformation. *J Geophys Res Solid Earth* 118:3059–3079. doi:10.1002/jgrb.50217
- Altamimi Z, Collilieux X, Legrand J et al (2007) ITRF2005: a new release of the international terrestrial reference frame based on time series of station positions and earth orientation parameters. *J Geophys Res Solid Earth* 112:B09401. doi:10.1029/2007JB004949
- Bevis M, Brown A (2014) Trajectory models and reference frames for crustal motion geodesy. *J Geod* 88:283–311. doi:10.1007/s00190-013-0685-5
- Drewes H (2009) The actual plate kinematic and crustal deformation model APKIM2005 as basis for a non-rotating ITRF. In: Geodetic reference frames. Springer, Berlin, pp 95–99
- Drewes H, Heidbach O (2012) The 2009 horizontal velocity field for South America and the Caribbean. In: Kenyon S, Pacino MC, Marti U (eds) *Geodesy for planet earth*. Springer, Berlin, pp 657–664
- Drewes H, Sánchez L (2013) Modelado de deformaciones sísmicas en el mantenimiento de marcos geodésicos de referencia. [http://www.sirgas.org/fileadmin/docs/Boletines/Bol18/36\\_Drewes\\_Sanchez\\_2013\\_Modelado\\_deformaciones\\_sismicas.pdf](http://www.sirgas.org/fileadmin/docs/Boletines/Bol18/36_Drewes_Sanchez_2013_Modelado_deformaciones_sismicas.pdf). Accessed 4 January 2014
- Drewes H, Sánchez L (2014) Actualización del modelo de velocidades SIRGAS. [http://www.sirgas.org/fileadmin/docs/Boletines/Bol19/60\\_Drewes\\_et\\_al\\_2014\\_ActualizacionVEMOS.pdf](http://www.sirgas.org/fileadmin/docs/Boletines/Bol19/60_Drewes_et_al_2014_ActualizacionVEMOS.pdf). Accessed 2 May 2015
- Dziewonski AM, Anderson DL (1981) Preliminary reference Earth model. *Phys Earth Planet Inter* 25:297–356
- Gómez D, Smalley R, Langston C et al (2015) Co-seismic deformation of the 2010 Maule, Chile earthquake: validating a least squares collocation interpolation. *GeoActa* 40(1), 25–35
- Hayes GP, Wald DJ, Johnson RL (2012) Slab1.0: a three-dimensional model of global subduction zone geometries. *J Geophys Res Solid Earth* 117:2012JB008524. doi:10.1029/2011JB008524
- Hu Y, Wang K, He J et al (2004) Three-dimensional viscoelastic finite element model for postseismic deformation of the great 1960 Chile earthquake. *J Geophys Res Solid Earth* 109:B12403. doi:10.1029/2004JB003163
- Khazaradze G, Wang K, Klotz J et al (2002) Prolonged post-seismic deformation of the 1960 great Chile earthquake and implications for mantle rheology. *Geophys Res Lett* 29:7–1
- Ligas M, Kulczycki M (2010) Simple spatial prediction-least squares prediction, simple kriging, and conditional expectation of normal vector. *Geod Cartogr* 59:69–81
- Lin YN, Sladen A, Ortega-Culaciati F et al (2013) Coseismic and post-seismic slip associated with the 2010 Maule earthquake, Chile: characterizing the Arauco Peninsula barrier effect: characterizing Arauco barrier effect. *J Geophys Res Solid Earth* 118:3142–3159. doi:10.1002/jgrb.50207
- Lorito S, Romano F, Atzori S et al (2011) Limited overlap between the seismic gap and coseismic slip of the great 2010 Chile earthquake. *Nat Geosci* 4:173–177. doi:10.1038/ngeo1073
- Maerten F (2005) Inverting for slip on three-dimensional fault surfaces using angular dislocations. *Bull Seismol Soc Am* 95:1654–1665. doi:10.1785/0120030181
- Moreno M, Melnick D, Rosenau M et al (2012) Toward understanding tectonic control on the Mw 8.8 2010 Maule Chile earthquake. *Earth Planet Sci Lett* 321–322:152–165. doi:10.1016/j.epsl.2012.01.006
- Okada Y (1985) Surface deformation due to shear and tensile faults in a half-space. *Bull Seismol Soc Am* 75:1135–1154
- Pollitz FF (1996) Coseismic deformation from earthquake faulting on a layered spherical Earth. *Geophys J Int* 125:1–14
- Pollitz FF, Brooks B, Tong X et al (2011) Coseismic slip distribution of the February 27, 2010 Mw 8.8 Maule, Chile earthquake: Chile earthquake coseismic slip. *Geophys Res Lett* 38. doi:10.1029/2011GL047065
- Seemüller W, Seitz M, Sánchez L, Drewes H (2009) The position and velocity solution SIR09P01 of the IGS Regional Network Associate Analysis Centre for SIRGAS (IGS RNAAC SIR). Munich Ger Dtsch Geod Forschungsinstitut Rep 85:96
- Snay RA, Freymueller JT, Pearson C (2013) Crustal motion models developed for version 3.2 of the horizontal time-dependent positioning utility. *J Appl Geod*. doi:10.1515/jag-2013-0005
- Tong X, Sandwell D, Luttrell K, et al (2010) The 2010 Maule, Chile earthquake: downdip rupture limit revealed by space geodesy: downdip rupture maule, Chile earthquake. *Geophys Res Lett* 37. doi:10.1029/2010GL045805
- Vieira SR, de Carvalho JRP, Ceddia MB, González AP (2010) Detrending non stationary data for geostatistical applications. *Bragantia* 69:01–08
- Wang K, Hu Y, Bevis M et al (2007) Crustal motion in the zone of the 1960 Chile earthquake: detangling earthquake-cycle deformation and forearc-sliver translation. *Geochem Geophys Geosyst* 8:Q10010. doi:10.1029/2007GC001721
- Wessel P, Smith WH (1998) New, improved version of generic mapping tools released. *Eos Trans Am Geophys Union* 79:579–579
- Zweck C, Freymueller JT, Cohen SC (2002) Three-dimensional elastic dislocation modeling of the postseismic response to the 1964 Alaska earthquake. *J Geophys Res Solid Earth* 107:ECV-1